Structural Peculiarities of Mesostructured Carbons Obtained by Nanocasting Ordered Mesoporous Templates via Carbon Chemical Vapor or Liquid Phase Infiltration Routes

Julien Parmentier,*,† Leonid A. Solovyov,*,‡ Françoise Ehrburger-Dolle,§ Jacques Werckmann,|| Ovidiu Ersen,|| Françoise Bley,⊥ and Joël Patarin†

Laboratoire de Matériaux à Porosité Contrôlée, Ecole Nationale Supérieure de Chimie de Mulhouse, UMR CNRS 7016, Université de Haute Alsace, 3 rue Alfred Werner, 68093 Mulhouse Cedex, France, Institute of Chemistry and Chemical Technology, K. Marx av. 42, 660049 Krasnoyarsk, Russia, Laboratoire de Spectrométrie Physique, UMR 5588 CNRS - UJF, Domaine Universitaire, BP 87, 38402 Saint Martin d'Hères cedex, France, Institut de Physique et de Chimie des Matériaux de Strasbourg, UMR 7504 CNRS - ULP, 23 rue du Loess, 67037 Strasbourg Cedex, France, and Laboratoire de Thermodynamique et Physico-Chimie Métallurgiques, UMR 5614 CNRS-UJF-INPG, Domaine Universitaire, BP 75, 38402 Saint-Martin d'Hères cedex, France

Received June 19, 2006. Revised Manuscript Received September 27, 2006

Mesostructured carbon materials were obtained by nanocasting MCM-48 and SBA-15 ordered mesoporous silica templates via two carbon infiltration routes: a liquid-phase process (LPI) using sucrose solution or a gas-phase chemical vapor infiltration (CVI) process using propene. The structural characteristics of the carbon replicas were investigated by synchrotron low-angle X-ray diffraction (LAXRD) analysis in combination with transmission electron microscopy (TEM). The materials obtained by the liquid-phase process demonstrated a long-range mesoscopic order at relatively low carbon loading (ca. 35 wt % in SiO_2/C composite), with their structural elements being essentially shrunk compared to that of the templates. The CVI replicas at similar low infiltration content were found to be only partly organized within nanodomains, but at bigger carbon loading (ca. 50 wt %) highly ordered mesostructures displaying up to ten nonzero XRD reflections were obtained. Moreover, these materials were shown to have thicker frameworks faithfully replicating their templates. Particular features of the CVI replica of MCM-48 were an amorphous carbon shell on the external particle surface and a gradient of the nanoframework displacement. The carbon replicas of SBA-15 were characterized by a semitubular structure.

Introduction

The control of porosity for porous carbon materials is a breakthrough challenge for the carbon research community. Different processes were developed to tailor the pore size distribution[1] either in the micro- or mesoporous ranges. Among them, the activation of carbon by a physical or chemical route is the most common procedure since activated carbons are of major industrial significance as adsorbents for their highly developed internal surface area and porosity. Despite tremendous efforts devoted to the development of preparative methods, strict control of the pore structure of activated carbons is still unavailable. An alternative route consists of the use of a hard template, also called exo-template,[2] which is impregnated with carbon and then selectively removed by chemical etching. The resulting carbon replica displays, in principle, a reverse porosity of the starting host material. Numerous templates with controlled porosity have been tested for the preparation of carbon replicas by this nanocasting process using crystallized microporous compounds such as zeolites,[3] clays,[4] and mesoporous (organized or disordered) silicas.[5] The last type of materials are very versatile moulds since their synthesis is well-controlled and can lead to ordered mesoporous structures with a narrow pore size distribution over a large range (2−15 nm), controlled pore features (channel, cage), connectivity (one-dimensional (1D) or three-dimensional (3D)), symmetry, and tailored wall thickness. Moreover, the resulting mesoporous carbon replicas may display high

* Corresponding authors. J. Parmentier: e-mail, Julien.Parmentier@univ-mulhouse.fr; phone, +33 (0) 3 89 33 68 87; fax, +33 (0) 3 89 33 68 85. L. A. Solovyov: e-mail: leosol@icct.ru.

† UMR CNRS 7016, Université de Haute Alsace.

‡ Institute of Chemistry and Chemical Technology.

§ UMR 5588 CNRS - UJF, Domaine Universitaire.

|| Institut de Physique et de Chimie des Matériaux de Strasbourg, UMR 7504 CNRS - ULP.

⊥ UMR 5614 CNRS-UJF-INPG, Domaine Universitaire.

(1) Kyotani, T. *Carbon* **2000**, *38*, 269.

(2) Schüth, F. *Angew. Chem., Int. Ed.* **2003**, *42*, 3604.

(3) (a) Kyotani, T.; Nagai, T.; Inoue, S.; Tomita, A. *Chem. Mater.* **1997**, *9*, 609. (b) Sonobe, N.; Kyotani, T.; Tomita, A. *Carbon* **1991**, *29*, 61. (c) Kyotani, T.; Mori, T.; Tomita, A. *Chem. Mater.* **1994**, *6*, 2138. (d) Bandosz, T.; Putyera, K.; Schwarz, J. A. *Carbon* **1994**, *32*, 659. (e) Bandosz, T.; Jagiello, J.; Putyera, K.; Schwartz, J. A. *Langmuir* **1995**, *11*, 3964. (f) Kyotani, T.; Ma, Z.; Tomita, A. *Carbon* **2003,** *41*, 1451. (g) Kyotani, T.; Nagai, T.; Inoue, S.; Tomita, A. *Chem. Mater.* **1997**, *9*, 609.

(4) (a) Kyotani, T.; Sonobe, N.; Tomita, A. *Nature* **1988**, *331*, 331. (b) Barata-rodrigues, P. M.; Mays, T. J.; Moggridge, G. D. *Carbon* **2003**, *41*, 2231.

(5) (a) Ryoo, R.; Joo, S. H.; Jun, S. *J. Phys. Chem. B* **1999,** *103*, 7743. (b) Yang, H.; Zhao, D. *J. Mater. Chem.* **2005**, *15*, 1217. (c) Gierszal, K. P.; Kim, T. -W.; Ryoo, R.; Jaroniec, M. *J. Phys. Chem. B* **2005**, *109*, 23263.

10.1021/cm061418k CCC: $33.50
Published on Web 11/22/2006

specific surface areas (up to 1800 m^2/g) and pore volume (up to 1.5 cm^3/g) that make them attractive candidates for potential applications as energy storage materials and electrodes for supercapacitors.[6] Among the templates, MCM-48[7] and SBA-15[8] are the most extensively used materials for the preparation of organized mesoporous carbons (OMC) by nanocasting.

In this study, these two templates were selected because of their different porous characteristics, symmetry, and specific structural transformation of respective carbon replicas (see below). Moreover, the existence of an ordering of the porosity makes also these materials attractive as model objects for studying their physicochemical properties and those of their carbon replicas. It is worth noting that the influence of carbon precursor on the final properties of carbon replica is often described in the literature, but in-depth studies of the infiltration mechanism and peculiar features related to the precursors (liquid or gaseous) are barely reported. Here we present detailed low-angle X-ray diffraction (LAXRD) and transmission electron microscopy (TEM) structural investigations of a series of ordered mesoporous carbons. These materials were obtained by nanocasting via chemical vapor infiltration (CVI) and liquid phase infiltration (LPI) of the above-mentioned templates. The geometric characteristics of the carbon replicas determined from LAXRD structural modeling are compared and discussed with those revealed by TEM. The information obtained gives explanations to the differences in the structural characteristics of the CVI and LPI carbon materials and to the process of their formation. A tentative description of the infiltration mechanism according to the carbon nanocasting route is presented. The adsorption characteristics of the ordered mesostructured carbon materials will be reported elsewhere.

Experimental Section

Description of Templates and Their Replication. MCM-48 mesoporous silica matrix has a three-dimensionally ordered cubic pore system with $Ia\bar{3}d$ symmetry space group.[7] It is composed of two interwoven non-interconnecting porous networks forming an enantiomeric pair. This bicontinuous periodic structure can be approximated by a triply periodic minimal surface called in that case also Gyroid minimal surface.[9] The corresponding carbon replicas obtained with sucrose,[10] divinylbenzene,[11] pitch,[12] and phenolic resin[13] as liquid carbon precursors display an ordered cubic structure with shrunk lattice and lower symmetry (space group $I4_1/a$ or lower).[10,14] The latter fact was revealed from LAXRD powder patterns due to the appearance of a strong low-angle diffraction peak (indexed as 110) that was related to the transformation of the mesostructure after the dissolution of the template wall. Further studies using TEM and LAXRD structural modeling showed that the enantiomeric carbon subframeworks formed within the pores of the MCM-48 template were homogeneously displaced with respect to one another without significant distortions after the dissolution of the silica wall of the template.[14,15] The structural modification led to the decrease of symmetry and to the appearance of the (110) XRD peak. This feature was confirmed by the use of partially disorganized MCM-48 templates with interconnecting micropores between the two interwoven pore networks.[16] In that case, the infiltration of micropores with carbon led to the formation of connecting bridges between the carbon subframeworks, which prevented their displacement; the cubic $Ia\bar{3}d$ space group of the MCM-48 was retained and no (110) XRD peak could then be detected.

The SBA-15 silica matrix presents a hexagonal array of mesopores interconnected by disordered micropores, leading to a three-dimensional porous structure that can be templated into ordered mesoporous carbon replicas.[17] According to the nanocasting process conditions and due to the larger pore size (above 5 nm) of SBA-15 compared to that of MCM-48, both volume and surface templating can be achieved that yield ordered carbon materials formed of either rod-type or tube-type structures, respectively. In the case of sufficient carbon content infiltrated (e.g., sucrose,[18] or 2 cycles of furfuryl alcohol impregnation,[19] or a long chemical vapor deposition[20]) the carbon material is formed of nanorods. The tube-type morphology can be achieved under more specific conditions, with a lower carbon content (e.g., a single furfuryl impregnation or a short-time chemical vapor deposition), a preliminary catalyst deposited onto the silica mesopore surface, or in a specific carbonization atmosphere. For instance, carbon nanopipes were obtained by carbonizing a polymerized furfuryl alcohol precursor under vacuum[21] (the ordered material was then denoted as CMK-5), or via a cobalt-catalyzed chemical vapor deposition of carbon using ethene.[20] Carbon replicas intermediate between nanorods and nanopipes were also obtained using a single furfuryl alcohol infiltration followed by carbonization under nitrogen instead of in vacuum.[19] The peculiar feature of LAXRD patterns of carbon nanopipe replicas is the inverse ratio between the intensity of reflections (10) and (11) attributed to the internal structure of these materials.[22]

Materials. MCM-48 silica material was prepared according to the procedure described by Schumacher et al.[23] and Kim et al.[24]

(6) (a) Lee, J.; Yoon, S.; Hyeon, T.; Oh, S. M.; Kim, K. B. *Chem. Commun.* **1999**, 2177. (b) Vix-Guterl, C.; Saadallah, S.; Frackowiak, E.; Jurewicz, K.; Reda, M.; Parmentier, J.; Patarin, J.; Béguin, F. *Mater. Sci. Eng. B* **2004**, *108*, 148. (c) Jurewicz, K.; Vix-Guterl, C.; Frackowiak, E.; Saadhallah, S.; Reda, M.; Parmentier, J.; Patarin, J.; Beguin, F. *J. Phys. Chem. Solids* **2004**, *65*, 287.
(7) Monnier, A.; Schüth, F.; Huo, Q.; Kumar, D.; Margolese, D.; Maxwell, R. S.; Stucky, G. D.; Krishnamurty, M.; Petroff, P.; Firouzi, A.; Janicke, M.; Chmelka, B. F. *Science* **1993**, *261*, 1299.
(8) Zhao, D.; Feng, J.; Huo, Q.; Melosh, N.; Frederickson, G. H.; Chemlka, B. F.; Stucky, G. D. *Science* **1998**, *279*, 548.
(9) Alfredsson, V.; Anderson, M. W. *Chem. Mater.* **1996**, *8*, 1141.
(10) Ryoo, R.; Joo, S. H.; Jun, S. *J. Phys. Chem B* **1999**, *103*, 7743.
(11) Yoon, S. B.; Kim, J. Y.; Yu, J.-S. *Chem. Commun.* **2001**, 559.
(12) Vix-Guterl, C.; Saadhallah, S.; Vidal, L.; Reda, M.; Parmentier, J.; Patarin, J. *J. Mater. Chem.* **2003**, *13*, 2535.
(13) Lee, J.; Yoon, S.; Hyeo, T.; Oh, S. M.; Kim, K. B. *Chem. Commun.* **1999**, 2177.
(14) Solovyov, L. A.; Zaikovskii, V. I.; Shmakov, A. N.; Belousov, O. V.; Ryoo, R. *J. Phys. Chem. B* **2002**, *106*, 12198.
(15) Kaneda, M.; Tsubakiyama, T.; Carlsson, A.; Sakamoto, Y.; Ohsuna, T.; Terasaki, O.; Joo, S. H.; Ryoo, R. *J. Phys. Chem. B* **2002**, *106*, 1256.
(16) Yang, H.; Shi, Q.; Liu, X.; Xie, S.; Jiang, D.; Zhang, F.; Yu, C.; Tu, B.; Zhao, D. *Chem. Commun.* **2002**, 2842.
(17) Ryoo, R.; Ko, C. H.; Kruk, M.; Antochshuk, V.; Jaroniec, M. *J. Phys. Chem. B* **2000**, *104*, 11465.
(18) Jun, S.; Joo, S. H.; Ryoo, R.; Kruk, M.; Jaroniec, M.; Liu, Z.; Ohsuna, T.; Terasaki, O. *J. Am. Chem. Soc.* **2000**, *122*, 10712.
(19) Fuertes, A. B. *Microporous Mesoporous Mater.* **2004**, *67*, 273.
(20) Zhang, W.-H.; Liang, C.; Sun, H.; Shen, Z.; Guan, Y.; Ying, P.; Li, C. *Adv. Mater.* **2002**, *14*, 1776.
(21) Joo, S. H.; Choi, S. J.; Oh, I.; Kwak, J.; Liu, Z.; Terasaki, O.; Ryoo, R. *Nature* **2001**, *412*, 169.
(22) Solovyov, L. A.; Kim, T.-W.; Kleitz, F.; Terasaki, O.; Ryoo, R. *Chem. Mater.* **2004**, *16*, 2274.
(23) Schumacher, K.; Von Hohenesche, C.; Unger, K. K.; Ulrich, R.; Du Chesne, A.; Wiesner, U.; Spiess, H. W. *Adv. Mater.* **1999**, *11*, 1194.
(24) Kim, J.-M.; Kim, S.-K.; Ryoo, R. *Chem. Commun.* **1998**, 259.

SBA-15 was synthesized at 353 K using the process detailed by Galarneau et al.[25] The as-made materials were calcined in air at 823 K for 6 h to remove the organic species occluded in the pores. Both matrixes were infiltrated by LPI or CVI using a sucrose solution or propene, respectively. The former impregnation method (LPI) was the one described by Ryoo et al.[10] Briefly, the silica matrixes were impregnated twice with a sucrose solution containing the maximum quantity of sucrose allowed by the pore volume of the inorganic template. After the sucrose carbonization (1173 K for 3 h under vacuum), the carbon represented around 35 wt % in the SiO_2/C composite material, both templates having similar pore volume ($\sim$1 cm^3/g). In the second method (CVI) described elsewhere,[26] the silica templates were placed in a horizontal reactor and put into contact with propene (2.5 vol % in an argon flow) at 1020 K. The duration of the carbon deposition varied from 10 to 24 h for the carbon content from 20 up to 50 wt % in the SiO_2/C materials. The carbon content in the SiO_2/C composites was determined by thermogravimetry in air. For all SiO_2/C composites, the carbon materials were collected after the dissolution of the silica matrix in HF. EDX analysis indicated that no silica remained in the carbon material after the HF treatment. The carbon replicas thus obtained are denoted $C_{template-precursor-wt\%\ of\ carbon}$.

Characterization Methods. TEM studies were performed on a TOPCON-002B microscope with acceleration voltage of 200 kV. The samples were dispersed in ethanol using ultrasonic method and the suspension was subsequently dropped onto a copper grid recovered by a carbon thin layer. To obtain a better and more realistic image of the carbon replicas, some analyses were done on thin sections obtained by cutting the sample with an ultramicrotome.

Low-angle XRD measurements were performed on the French CRG beamline D2AM at the European Synchrotron Radiation Facility (ESRF) in Grenoble (France). Details about experimental setup and about data analysis were given in a previous paper.[27] In the present case, the domain of q-values,

$$q = \frac{4\pi \sin(\theta/2)}{\lambda}$$

where θ and λ are the scattering angle and the X-ray wavelength, respectively, ranges between ca. 0.5 and 10 nm^{-1}. In order for the width of the Bragg peaks to not be controlled by that of the incident X-ray beam, it is necessary to adjust the beam optics for obtaining a narrow spot. High peak resolution is achieved by selecting λ and sample-to-detector distance L_{s-d} to optimal values. For the MCM-48 silica and its corresponding carbon replicas, the Bragg peaks are located between ca. 1 and 5 nm^{-1}. For these samples, the X-ray wavelength λ was fixed to 0.077 nm (energy equal to 16 keV) and L_{s-d} was equal to 0.28 m. Under such conditions, the uncertainty ($\pm$1 pixel) on the position of the (211) peak (obtained by azimuthal averaging of the powder pattern measured by a CCD camera) corresponds to $\pm 1.25 \times 10^{-2}$ nm^{-1} and to $d \pm 0.03$ nm in the real space. For the (110) peak observed for the carbon replicas, the uncertainty on d ($=2\pi/q$) is $\pm$ 0.07 nm. The Bragg peaks of SBA-15 silica and its carbon replicas are located at smaller q-values (0.4−3.5 nm^{-1}). For investigating these samples, λ was fixed to 0.1 nm (E = 12.4 keV) and L_{s-d} = 0.81 m. Uncertainty on the position d of the (110) peak ($\pm$1 pixel, corresponding to $\pm 3.9 \times 10^{-3}$ nm^{-1}) is equal to $\pm$0.05 nm.

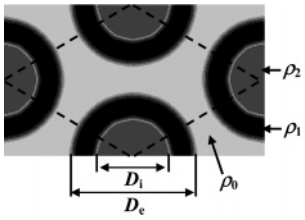

Figure 1. Model of density distribution for CVI carbon replica of SBA-15. The hexagonal unit cell is outlined by dashed lines.

The LAXRD structure analysis of the materials was done by applying the continuous density function (CDF) technique.[28] The diffraction patterns were modeled by using the Rietveld full-profile approach.[29] The refinement of structural parameters was performed by the derivative difference minimization (DDM) method,[30] which allowed concentrating the refinement on the pure Bragg-diffraction component independently of the amorphous background scattering modulations. The integrated diffraction intensities for the Fourier density map calculations were extracted from the observed LAXRD patterns by the DDM decomposition procedure.[31] The phases necessary for the Fourier maps were derived from the refined structure models. The internal structural disorder was allowed for by applying the Debye−Waller factor. For each type of template, the structure models were built to take into account their specific features.

The structure of the SBA-15 template was described by a simple model of empty pores and continuous walls similar to that applied to calcined MCM-41 mesoporous materials.[28] The variable structure parameters were the lattice constant, the pore diameter, the pore shape (degree of hexagonality),[28] and the Debye−Waller factor. For MCM-48 silica template and its carbon replicas the density distribution functions were chosen as described in ref 32 (eq 2) and ref 14, respectively.

For the CVI carbon replicas of SBA-15, the attempts of modeling the structures by the array of uniformly filled carbon nanorods, as was previously done for CMK-1,[36] did not allow for achieving satisfactory agreement between the observed and calculated LAXRD patterns. The Fourier-map analysis revealed distinct density minima in the centers of the carbon nanorods. To allow for this feature, the density distribution in this material was approximated by a more complex model function schematized in Figure 1. The structure is based on a hexagonal arrangement of carbon quasi-nanopipes (QNP) with high-density peripheral and core areas ρ_1 and ρ_2 characterized by the internal and external diameters D_i and D_e. These carbon nanostructures are separated by a region of lower density ρ_0 representing the interconnections formed in the complementary pores inside the SBA-15 template walls. The variable parameters were the lattice constant, the diameters D_i and D_e, the ratio $(\rho_0 + \rho_2)/(\rho_0 + \rho_1)$, the QNP shape hexagonality, and the Debye−Waller factor. Unlike the nanopipe mesostructured carbons CMK-5,[21,22] the density of interconnections ρ_0 could not be explicitly determined for the studied carbon materials since they do not have zero density regions required as reference points. For the LPI replica of SBA-15, the above-described quasi-pipe features were not found and the density distribution was modeled by a simplified function with $\rho_1 = \rho_2$.

(25) (a) Galarneau, A.; Cambon, H.; Di Renzo, F.; Ryoo, R.; Choi, M.; Fajula, F. *New J. Chem.* **2003**, *27*, 73. (b) Galarneau, A.; Cambon, H.; Di Renzo, F.; Fajula, F. *Langmuir* **2001**, *17*, 8328.
(26) Parmentier, J.; Patarin, J.; Dentzer, J.; Vix-Guterl, C. *Ceram. Int.* **2002**, *28*, 1.
(27) Ehrburger-Dolle, F.; Morfin, I.; Geissler, E.; Bley, F.; Livet, F.; Vix-Guterl, C.; Saadhallah, S.; Parmentier, J.; Reda, M.; Patarin, J.; Illescu, M.; Werckmann, J. *Langmuir* **2003**, *19*, 4303 .
(28) (a) Solovyov, L. A.; Kirik, S. D.; Shmakov, A. N.; Romannikov, V. N. *Microporous Mesoporous Mater.* **2001**, *44-45*, 17. (b) Solovyov, L. A.; Kirik, S. D.; Shmakov, A. N.; Romannikov, V. N. *Adv. X-ray Anal.* **2001**, *44*, 110.
(29) Rietveld, H. M. *J. Appl. Crystallogr.* **1969**, *2*, 65.
(30) Solovyov, L. A. *J. Appl. Crystallogr.* **2004**, *37*, 743.
(31) Solovyov, L. A.; Astachov, A. M.; Molokeev, M. S.; Vasiliev, A. D. *Acta Crystallogr. B* **2005**, *61*, 435.

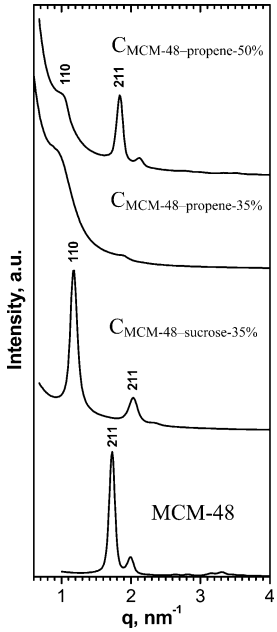

Figure 2. LAXRD patterns of MCM-48 and its carbon replicas obtained with sucrose and propene precursors.

Results and Discussion

The various influences of both preparation routes (CVI and LPI) on the structural properties of the resulting carbon materials were explored by nanocasting MCM-48 and SBA-15 templates. The LAXRD patterns of MCM-48 and its replicas are shown in Figure 2. The patterns demonstrate noticeable differences in both positions and intensities of diffraction peaks. For sample $C_{MCM-48-sucrose-35\%}$, the (110) XRD peak is well-resolved and is more intense than the (211) peak. Moreover, the LAXRD pattern is considerably shifted with respect to that of MCM-48 due to the lattice shrinkage. These features are characteristic of ex-sucrose carbon replicas of MCM-48 (see Experimental Section). When propene is used as carbon precursor, the pattern of the carbon replica obtained with a similar carbon filling (35 wt %) exhibits only two shallow maxima in the regions of the (110) and (211) reflection positions. At a higher carbon loading (50 wt %), the (211) and higher angle reflections are well-resolved whereas the (110) reflection still remains weak and broad.

The TEM micrograph of the $C_{MCM-48-propene-35\%}$ sample (Figure 3) clearly reveals the existence of nanodomains (ca. 30 nm in size) with a local mesoscale ordering derived from the template. The Fourier transform pattern of this image (inset in Figure 3) indicates that these domains are generally coherent. The poorly resolved XRD pattern of the $C_{MCM-48-propene-35\%}$ sample results, therefore, from the size-induced broadening effect and the semiordering of nanodomains. These features do not appear for the sucrose process with similar carbon filling because LPI is achieved through the entire template porosity, leading to continuous carbon frameworks and, therefore, to long-range ordering. With the increase of the carbon content in the CVI process, the coherent organized domains grow and overlap; a resulting long-range ordering is then obtained, as revealed by the LAXRD pattern of sample $C_{MCM-48-propene-50\%}$ (Figure 2).

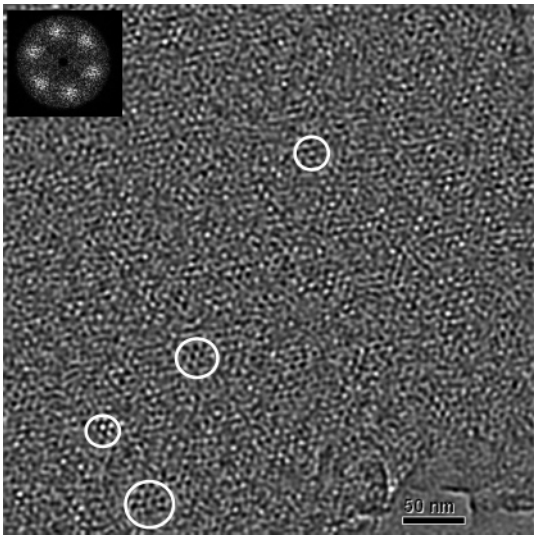

Figure 3. TEM micrograph of ultramicrotome section of sample $C_{MCM-48-propene-35\%}$ showing nanodomains with local ordering (view along the [111] direction). The inset represents the Fourier transform of the image. The six spots on the Fourier diffractogram correspond to 110-type reflections from the highly distorted and randomly displaced carbon framework.

Further details of the materials structure were derived from the LAXRD analysis. The results of the full-profile DDM refinement of the structures of MCM-48 silica template and its CVI and LPI carbon replicas are illustrated by Figure 4. This figure demonstrates a fair consistency between the observed and calculated LAXRD patterns. The resultant structural parameters are summarized in Table 1. For MCM-48, the calculated wall thickness is 0.81 nm and the relative density increase between high- and low-curvature pore wall regions is refined to a value of 11%, which fully agrees with results obtained in an earlier investigation for analogous materials.[32] The diffraction peak resolution is similar for the CVI carbon replica ($C_{MCM-48-propene-50\%}$) and its silica template. It may thus be assumed that CVI yields a nearly nondistorted carbon replica. The pattern obtained for the LPI replica ($C_{MCM-48-sucrose-35\%}$) is less resolved, which points to a larger structural distortion. Nevertheless, owing to the high resolution, high intensity, and properly adjusted wavelength of the synchrotron setup, up to eight nonzero reflections can be observed. The structure refinement for the LPI ex-sucrose carbon replica reveals that its framework thickness (2.64 nm) is notably smaller than the estimated template pore diameter (3.64 nm). Also, the value of the mutual subframework displacement (1.29 nm) exceeds the template wall thickness. Similar features were observed for a sucrose-based carbon replica of MCM-48 in earlier research.[14] In contrast, the framework thickness of the CVI carbon replica is close to the template pore diameter and the subframework displacement is even smaller than the silica wall thickness (which will be discussed later). Indeed, the low carbon filling with LPI (35 wt %) leads to carbon frameworks that are thinner than those obtained by CVI (50 wt %). Furthermore, these weak frameworks were subjected to a higher temperature treatment (1173 K) compared to those of the CVI process (1023 K). Thus, the LPI-derived carbon

(32) Solovyov, L. A.; Belousov, O. V.; Dinnebier, R. E.; Shmakov, A. N.; Kirik, S. D. *J. Phys. Chem. B* **2005**, *109*, 3233.

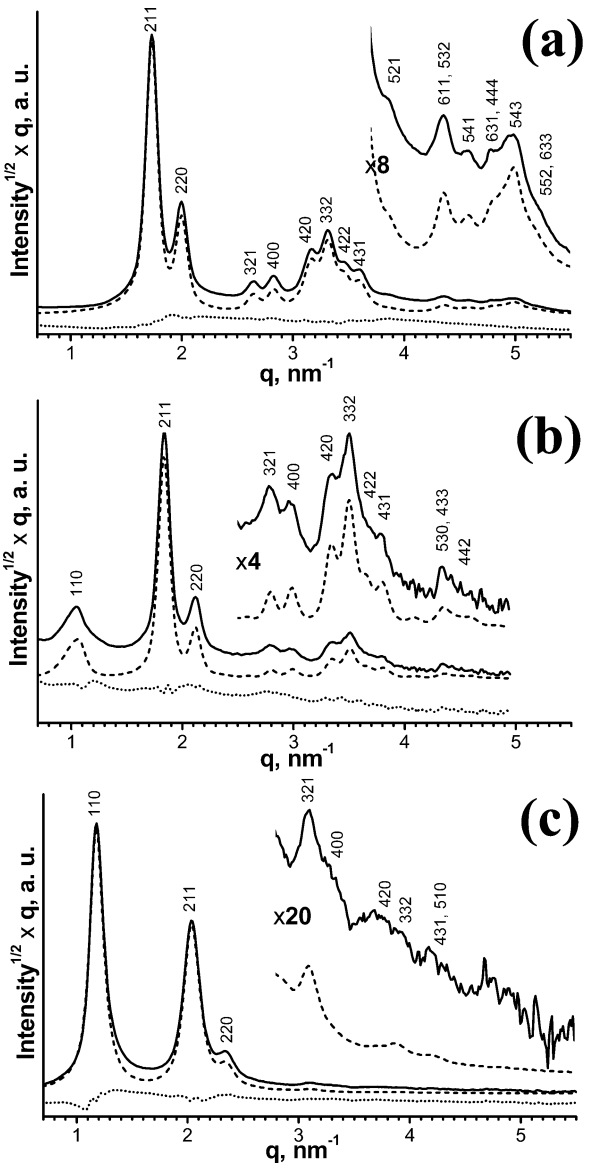

Figure 4. Weighted and Lorenz-factor corrected observed (solid line), calculated (dashed line), and difference (dotted line) LAXRD patterns for samples MCM-48 (a), $C_{MCM-48-propene-50\%}$ (b), and $C_{MCM-48-sucrose-35\%}$ (c) after CDF−DDM structure refinement.

Table 1. Structural Parameters Obtained by CDF−DDM Refinement from LAXRD Data for MCM-48 Silica and Its Carbon Replicas[a]

sample	*a*, nm	*t* or *ft*, nm	*fd*, nm
MCM-48[b]	8.90	0.81	
$C_{MCM-48-propene-50\%}$	8.42	3.29	0.67
$C_{MCM-48-sucrose-35\%}$	7.58	2.64	1.29

[a] *a*, lattice parameter; *t*, silica wall thickness (for MCM-48); *ft*, framework thickness (for carbons) defined by eq 3 in ref 14; *fd*, average mutual displacement of the subframeworks. [b] The pore diameter of MCM-48 can be estimated as $a/2 - t = 3.64$ nm.

frameworks might be distorted more easily after the silica wall dissolution. Furthermore, during the carbonization step, the shrinkage of the sucrose precursor (73 vol %)[33] is significantly larger than that of the silica matrix (36 vol %).[34] It is likely that this large difference in shrinkage creates gaps between the carbon subframeworks and the silica walls. Such gaps might result in distorted and strained frameworks that could again be rearranged during silica dissolution. These features may explain the differences in the structural details of the LPI- and CVI-produced carbon materials.

Figure 4b also shows that the (110) XRD peak of the CVI carbon (sample $C_{MCM-48-propene-50\%}$) is substantially broadened in comparison with the other reflections. Analysis of the TEM image of that sample allows an explanation for this observation. Indeed, the micrography (Figure 5b) clearly shows that the particle is covered by a shell of amorphous carbon unlike the one prepared by LPI (Figure 5a). Moreover, two different TEM patterns are observed for the CVI sample: one in the region close to the external shell (Region A in Figure 5b) and the other in the interior of the particle (Region B). The TEM simulations performed on the basis of the structural model detailed in the Experimental Section for MCM-48 carbon replicas clearly suggest that the regions A and B correspond to the undisplaced and displaced carbon subframeworks, respectively (Figure 5c). Therefore, it may be concluded that the external amorphous carbon shell is rigidly bonded with the carbon subframeworks, which precludes their displacement at the vicinity of the outer surface. This effect diminishes as the distance from the surface increases, leading to a gradient in the framework displacement for region A and a relatively constant displacement in region B. The line profiles of angular averaged Fourier diffractograms for regions A and B are shown in Figure 6. These profiles demonstrate that a gradient of displacement (region A) induces the broadening of the (110) reflection which explains the similar feature observed in the XRD pattern for the $C_{MCM-48-propene-50\%}$ replica. This effect is analogous to the selective broadening of XRD peaks for crystalline materials containing structural defects.[35] The subframework displacement has a major effect on the intensity of the (110) reflection and a negligible effect on the remaining reflections. Due to the gradient of displacement, the coherent length (or size of regular structured domains), determining the XRD peak width, is decreased for the (110) reflection and remains nearly unchanged for the remaining reflections, in accordance with the generalized theory described in ref 35. In the case of LPI carbon replicas, the frameworks are displaced uniformly, owing to the absence of the outer amorphous shell, which accounts for the absence of the selective XRD peak broadening in this material.

The influence of the infiltration route on the structural characteristics of the carbon replicas is further analyzed by the study of the SBA-15 silica template and the corresponding ordered mesoporous carbon replicas obtained by LPI and CVI routes. Figure 7 shows that the low-angle setup used in the present experiment allows one to see up to 10 nonzero XRD reflections for the SBA-15 silica template, whereas only 3 or up to 5 XRD peaks have been generally observed for ordered nanorod and nanopipe carbons.[20,22,36,37]

As shown in Figure 7, the above-described density distribution models for SBA-15 and its carbon replicas allow

(33) Joo, S. H.; Jun, S.; Ryoo, R. *Microporous Mesoporous Mater.* **2001**, *153*, 44−45.
(34) Parmentier, J.; Vix-Guterl, C.; Gibot, P.; Reda, M.; Iliescu, M.; Werckmann, J.; Patarin, J. *Microporous Mesoporous Mater.* **2003**, *62*, 87.
(35) Solovyov, L. A. *J. Appl. Crystallogr.* **2000**, *33*, 338.

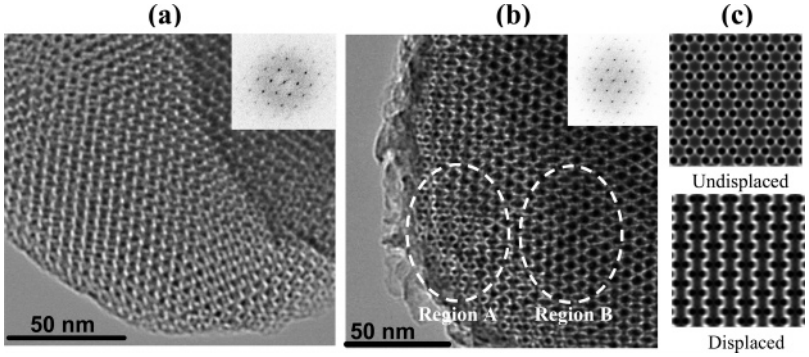

Figure 5. TEM micrographs of $C_{MCM-48-sucrose-35\%}$ (a) and $C_{MCM-48-propene-50\%}$ (b) samples viewed along the [111] direction and TEM simulations for undisplaced and displaced framework models (c). The simulations were made by projecting the density distribution function for a uniform (infinite) sample thickness onto a plane (the subframework displacement is 3.29 nm along [110]).

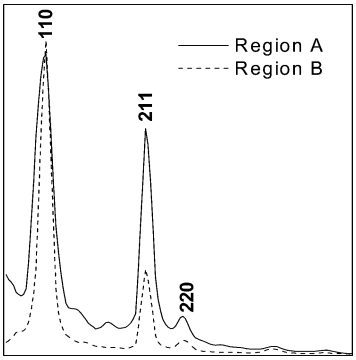

Figure 6. Line profiles of rotationally averaged Fourier diffractograms for regions A and B from the TEM image of Figure 5b.

a satisfactory CDF−DDM structure refinement for all the materials studied. The resulting structural parameters and the corresponding structure factors (observed and calculated) are listed in Table 2 and Table 3, respectively. The density distribution Fourier maps (based on observed structure factors and calculated phases) for the silica template and its carbon replicas are shown at the bottom of Figure 7. The analysis of difference Fourier maps did not reveal additional structure details such as the corona region in SBA-15[38] or other features. The structure refinement results show that the pores

Table 2. Structural Parameters of the SBA-15 Template and Its Carbon Replicas Determined from LAXRD by CDF−DDM Refinement[a]

sample	a, nm	D_e, nm	D_i, nm	$(\rho_0+\rho_2)/\rho_0+\rho_1)$	Hex, %
SBA-15	11.05	8.3			19
$C_{SBA-15-propene-50\%}$	10.52	8.0	3.6	0.82	23
$C_{SBA-15-sucrose-35\%}$	9.63	6.8	0[b]	1[b]	0[b]

[a] a, the lattice parameter; D_e, D_i, and $\rho_0...\rho_2$ are defined in Figure 1; Hex is the degree of hexagonality[28] of the mesopore (for SBA-15) or the quasi-nanorod shape. [b] These parameters were fixed.

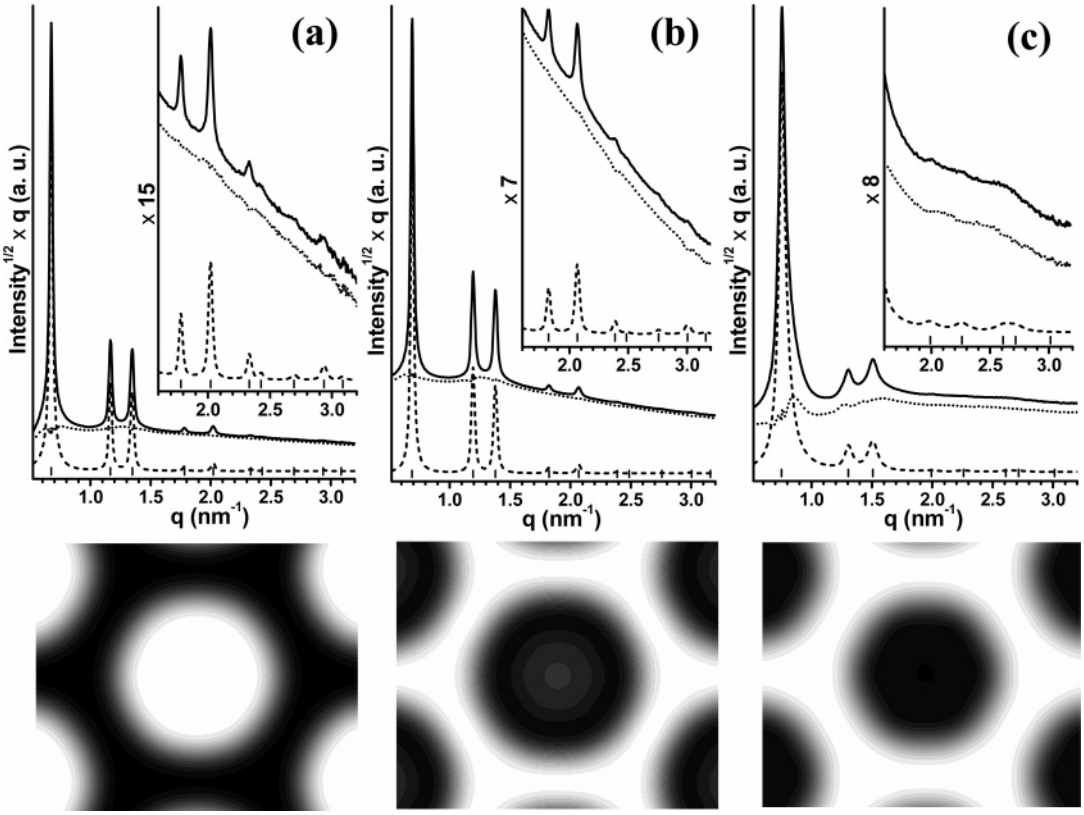

Figure 7. Weighted and Lorentz-factor corrected observed (solid line), calculated (dashed line), and difference (dotted line) LAXRD patterns after CDF−DDM refinement for samples SBA-15 (a), $C_{SBA-15-propene-50\%}$ (b), and $C_{SBA-15-sucrose-35\%}$ (c). Respective density distribution maps are shown at the bottom.

Table 3. Structure Factors (F_o) Derived from Observed LAXRD Patterns by DDM Decomposition in Comparison with Calculated Ones (F_c)[a]

	sample					
	SBA-15		$C_{SBA-15-propene-50\%}$		$C_{SBA-15-sucrose-35\%}$	
hk	$\|F_o\|$	F_c	$\|F_o\|$	F_c	$\|F_o\|$	F_c
01	100	−100.09	100	99.91	100	100.13
11	31.22	31.13	45.65	−45.80	20.11	−20.18
02	30.17	30.07	42.42	−42.21	26.23	−25.37
12	3.89	−3.88	6.64	6.59	2.19	−3.17
03	7.79	−7.84	12.07	11.82	3.38	4.97
22	3.14	−3.60	3.92	5.20	5.04	4.80
13	1.23	−1.23	1.41	1.32	3.06	3.41
04	1.45	1.75	2.63	−3.07		
23	1.67	1.99	2.22	−3.56		
14	0.95	0.92	0.58	−1.27		
R_F:	0.8%		2.1%		2.6%	

[a] R_F, the reliability factor characterizing the overall percent difference between the observed and calculated structure factor modules.

of SBA-15 are not perfectly cylindrical, but have some degree (ca. 20%) of shape hexagonality which is, however, much lower than that determined for MCM-41.[28,39]

Figure 7 also shows that the resolution of the XRD pattern obtained for the CVI carbon replica is better than that of the LPI one. This feature is an indication of the faithful replication of the SBA-15 template by the soft CVI process that also allows a high carbon filling into the mould (up to 50 wt %). Indeed, carbon deposition occurs at relatively low temperature (1023 K) that precludes a substantial shrinkage of the template. Therefore, the external diameter of the carbon framework D_e (8.0 nm) does not differ much from the pore diameter of its SBA-15 mould ($D_e = 8.3$ nm) and even the degree of the shape hexagonality is maintained in the replica.

The diameter D_i of the inner low-density quasi-nanorod region ρ_2 is quite large (3.6 nm) despite the high carbon loading (50 wt %) into the template. The XRD refinement and the Fourier map analysis show that the density ρ_2 of the inner region is far above zero. Since XRD gives information on an average structure, it may be concluded that this carbon framework has an internal structure in-between nanopipes and real nanorods. A similar explanation has already been proposed by Fuertes[19] in the case of liquid infiltration of furfuryl alcohol into SBA-15, followed by carbonization in a nitrogen atmosphere. The CVI process does not distinguish between the internal (pore) and the external particle surfaces. Therefore, carbon is deposited on both surfaces. For a low carbon filling, the replica exhibits probably a tubular structure poorly resolved due to the heterogeneity of the CVI process in the absence of a catalyst. This typical tubular structure was already reported by different authors as being resulted from a cobalt-catalyzed chemical vapor deposition route and only for low carbon loadings.[20] For higher amounts of infiltrated carbon, the same authors observed a progressive disappearance of the tubular structure in favor of the nanorod morphology. For our system, increasing the carbon content from 35 to 50 wt % might lead to thicker carbon layer (with local heterogeneities of the thickness) which reduces the remaining pore diameter and precludes diffusion of the carbonaceous gas species in the CVI process. Pores would be then blocked, embedding carbon tubular structures, while the remaining gas-accessible portion of mesopores would still be filled with carbon. The carbon framework would then consist of regions completely filled (nanorods) and regions partly filled displaying a tubular structure (nanopipes). A simple calculation in which the carbon filling is 50 wt %, the silica and carbon density is equal to 2.2 and 1.8 g/cm^3, respectively, and the silica pore volume is 0.95 cm^3/g indicates that only 60% of the template pore volume is filled by carbon. It means that a large part of the porosity (40%) remains unfilled in the SiO_2/C composite. Therefore, the carbon replica displays a porosity arising not only from the silica wall dissolution but also from unfilled regions due to a heterogeneous filling of the template or/and a tubular-like morphology. These assumptions are partly confirmed by TEM observations of a microtome section of the $C_{SBA-15-propene-50\%}$ sample (Figure 8) that give more details of the internal structure. Indeed, this micrograph indicates that the honeycomb structure contains numerous faults. These defects could be attributed, at least partly (besides effects of the ultra-microtome processing), to the heterogeneous and incomplete filling of the template. Thus, the internal structure of the material would consist of carbon nanorods (black circles) and carbon nanopipes (white circles) connected by bridges formed inside the connecting micropores of the template walls.

The LPI replica ($C_{SBA-15-sucrose-35\%}$) displays a less resolved XRD pattern compared to that of the CVI replica, $C_{SBA-15-propene-50\%}$. This feature may be explained, analogously to the $C_{MCM-48-sucrose-35\%}$ sample, by strong and heterogeneous distortions of the carbon framework during the nanocasting process. Indeed, the carbonization step takes place with a high contraction of the carbon precursor that is not totally accommodated by the silica matrix. Moreover, the necessity of a second sucrose infiltration to reach a sufficient carbon loading could lead to a heterogeneous filling due to the difficulty of infiltrating the previously partly filled mould. Thus, during carbonization, a strain gradient could be applied on the silica mould that leads to a decrease of the carbon replication quality. On the other hand, the high anisotropy of the SBA-15 structure compared to that of MCM-48 could enhance an anisotropic shrinkage within the carbon framework. For all these reasons, the LPI carbon replica displays a lower faithfulness to the template than the CVI one as it is revealed by the loss of long-range organization. The highly pronounced contraction of the carbon precursor is also shown by the difference between the diameter of the carbon nanorods D_e and the pore diameter of the SBA-15 template. This feature suggests, as for LPI in MCM-48, the existence of a gap between the silica and the carbon network. Residual modulations of the difference LAXRD profile after the DDM refinement for $C_{SBA-15-sucrose-35\%}$

(36) Solovyov, L. A.; Shmakov, A. N.; Zaikovskii, V. I.; Joo, S. H.; Ryoo, R. *Carbon* **2002**, *40*, 2477.
(37) Kruk, M.; Jaroniec, M.; Kim, T.-W.; Ryoo, R. *Chem. Mater.* **2003**, *15*, 2815.
(38) Imperor-Clerc, M.; Davidson, P.; Davidson, A. *J. Am. Chem. Soc.* **2000**, *122*, 11925.
(39) Solovyov, L. A.; Belousov, O. V.; Shmakov, A. N.; Zaikovskii, V. I.; Joo, S. H.; Ryoo, R.; Haddad, E.; Gedeon, A.; Kirik, S. D. *Stud. Surf. Sci. Catal.* **2003**, *146*, 299.

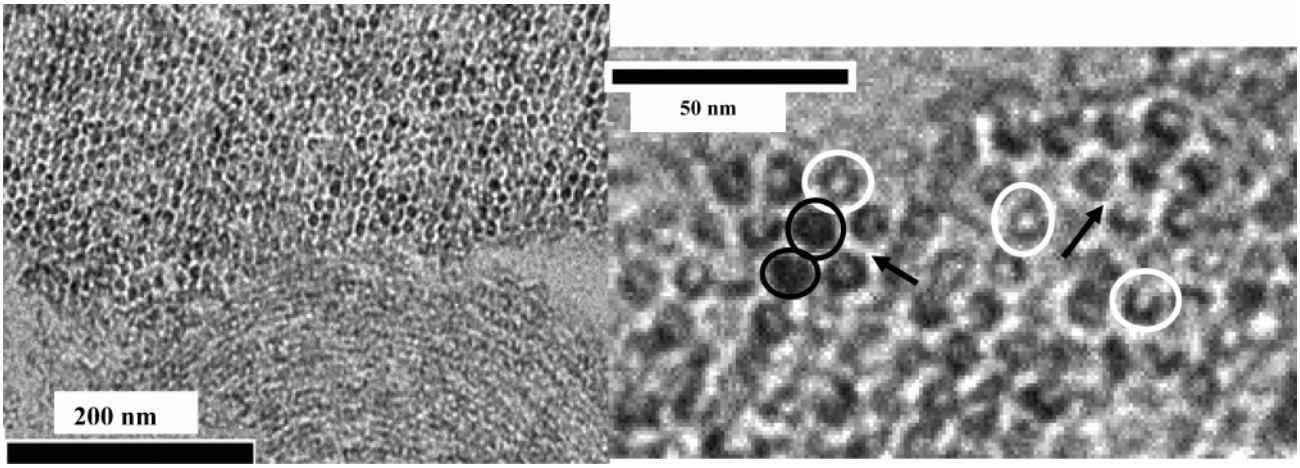

Figure 8. TEM micrographs of an ultra-microtome slice of $C_{SBA-15-propene-50\%}$ sample showing carbon rods (black circles), carbon tubules (white circles), and porosity arising from the silica wall dissolution (arrows).

(Figure 7c) may indicate also the presence of disordered and/or a distorted regions in the material.

Conclusions

The present work shows that carbon precursors and infiltration routes play a crucial role in the formation of carbon replica structures by influencing the mechanism of nanocasting. For the CVI process, the precursor does not distinguish between the internal and the external surface, which resulted in carbon deposition on both surfaces. For a low amount of the infiltrated precursor and in the absence of a catalyst, the carbon layer is discontinuous because carbon deposition takes place preferentially on active sites. As a result, the carbon replica exhibits only local organization, but the long-range ordering is disturbed. The LPI process fills the template mesopores more uniformly, leaving the external particle surface free of an amorphous shell. The carbon framework is then continuous with a long-range ordering, even if the amount of carbon precursor is low. By increasing the carbon content in the CVI route, a kind of percolation threshold is exceeded. Above this threshold, a continuous carbon replica with a long-range ordering can be obtained. For the CVI carbon replica of MCM-48 the existence of an external amorphous shell hinders the displacement of the carbon subframeworks after the silica wall dissolution, thus inducing a gradient of framework displacement. For the carbon replicas of both MCM-48 and SBA-15 templates the materials resulting from LPI display essentially shrunk and distorted structure with thinner framework elements compared to the CVI-based replicas. A particular feature of the CVI carbon replica of SBA-15 is a semitubular structure resulting, presumably, from the heterogeneous template infiltration.

Owing to the use of the high-resolution synchrotron low-angle XRD setup and the modern methods of continuous density function[28] and derivative difference minimization[30] in combination with TEM analysis, good quality data and comprehensive information about the structure of the investigated materials were obtained in the present work. Further investigations are required to completely explain the influence of carbon precursors on the porosity and anatomy of the nanocasted materials, and to propose a detailed mechanism of infiltration in relation to the experimentally observed features.

Acknowledgment. This work was supported by the grants of RFBR 03-03032127, the French Ministry of Research (ACI Nanostructure − Nanotechnologie 2002), and the CNRS (Programme Matériaux). We are grateful to C. Vix-Guterl for fruitful discussion, to the European Radiation Synchrotron Facility (ESRF, Grenoble, France) for beam time on BM2-D2AM, to the beamline staff, Jean-François Berar, Nathalie Boudet, Bernard Caillot, and Stephan Arnaud for technical assistance, and to Isabelle Morfin for her help in running LAXRD measurements.

CM061418K